COMMUN. MATH. SCI.
Vol. 21, No. 4, pp. 997–1018


# RESIDUAL-BASED A POSTERIORI ERROR ESTIMATION FOR ELLIPTIC INTERFACE PROBLEMS APPROXIMATED BY IMMERSED FINITE ELEMENT METHODS*

YANPING CHEN†, JIAO LU‡, YANG WANG§, AND YUNQING HUANG¶

**Abstract.** This paper studies a residual-based a posteriori error estimator for partially penalized immersed finite element (PPIFE) approximation to elliptic interface problems. Utilizing the error equation for the PPIFE approximation, we construct an a posteriori error estimator. Properly weighted coefficients are proposed for the terms in indicators to overcome the dependence of the efficiency constants on the jump of the diffusion coefficients across the interface. The PPIFE method is based on non-body-fitted mesh, and hence we perform detailed analysis on the local efficiency bounds of the estimator on regular and irregular interface elements with different techniques. We introduce a new approach, which does not involve the Helmholtz decomposition, to give the reliability bounds of the estimator with an $L^2$ representation of the true error as the main tool. More importantly, the efficiency and reliability constants are independent of the interface location and the mesh size. Numerical experiments are provided to illustrate the efficiency of the estimator and the adaptive mesh refinement for different jump rates or interface geometries.

**Keywords.** Interface problems; a posteriori error estimator; immersed finite element methods; adaptive refined meshes.

**AMS subject classifications.** 35R05; 65N15; 65N30.

## 1. Introduction

Interface problems with discontinuous coefficients have appeared widely in a variety of engineering and physical fields, for instance, stationary heat conduction problems with a discontinuous conduction coefficient [1], fluid problems with different viscosities [2], electromagnetic problems [3] and so on [4, 5]. Because of the discontinuity of the coefficients in the equation and the nature of the interface, the solution of the interface problem usually has low accuracy. As a result, it is a considerable challenge to solve interface problems efficiently and accurately.

There are some methods based on body-fitted grids available in the literature to solve interface problems, such as the classical finite element methods [6, 7], the virtual element methods [8, 9], and the weak Galerkin methods [10, 11]. These methods require the mesh to align with the interface to render a high-order accurate approximation (see Figure 1.1(c)). If the shape or location of the interface does not change, using these methods to solve problems is relatively efficient. However, it may be difficult and time-consuming to solve a problem with a moving or complex interface. Other methods based on structured grids that do not align with the interface have been developed, such as extended finite element methods [12, 13], immersed interface methods [14, 15], and immersed finite element methods [16–22]. These methods have many advantages

*Received: December 24, 2021; Accepted (in revised form): September 05, 2022. Communicated by Shi Jin.

†School of Mathematical Sciences, South China Normal University, Guangzhou, 510631, China (yanpingchen@scnu.edu.cn).

‡School of Mathematics and Computational Science, Xiangtan University, Xiangtan, 411105, Hunan, China (Stu_lujiao@163.com).

§School of Mathematics and Statistics, Hubei Normal University, Huangshi, 435002, China (wy2010ang@163.com).

¶School of Mathematics and Computational Science, Hunan Key Laboratory for Computation and Simulation in Science and Engineering, Xiangtan University, Xiangtan, 411105, Hunan, P.R. China (huangyq@xtu.edu.cn).

over the usual body-fitted grid methods. In particular, when a problem with a moving interface is involved, they do not need to generate a new grid as time evolves. This simplifies the solving process and saves a considerable amount of storage.

The immersed finite element (IFE) methods were first introduced by Li in [23] as a new finite element method for solving one-dimensional elliptic interface problems. The key to the IFE methods is to construct piecewise polynomials on interface elements according to interface jump conditions while using standard polynomials on non-interface elements. Subsequently, the partially penalized immersed finite element (PPIFE) method was proposed in [24]. This method adds extra stabilization terms on interface edges to penalize the discontinuity of the IFE functions and maintain the stability of the format. As a result, the accuracy near the interface is improved while maintaining the stability of the algorithm. More recently, the PPIFE method has been proposed for parabolic interface problems [25], hyperbolic interface problems [26], elasticity interface problems [27, 28], and so on [29, 30].

Since IFE functions are discontinuous over interface elements, the IFE methods often have a much larger error near the interface. This indicates that IFE solution errors are not uniformly distributed throughout the solution region. Therefore, if we simply improve numerical approximation accuracy by using a global uniform refined grid, it is computationally expensive and cannot accurately refine the regions with large errors. We consider introducing an adaptive refinement strategy based on a posteriori error estimation. The strategy uses the information from the IFE solution computed on some initially uniform mesh and then adapts the grid in a post-processing way, thereby obtaining a grid more tailored to the problem. Moreover, the adaptive strategy reduces the number of unknowns and can converge to the exact solution faster. A posteriori error indicators in the adaptive refinement process provide vital information for generating a new refined mesh. Over the past six years, the residual-based a posteriori error estimate analysis for IFE methods has been less studied, and only a few results have been attained so far. Chen et al. [31] proposed an adaptive IFE method with error control by introducing different error indicators on interface elements and non-interface elements, respectively, which can effectively solve elliptic and Maxwell interface problems. He and Zhang [32] analyzed a residual-based posterior error estimate for the PPIFE method for elliptic interface problems and then used the Helmholtz decomposition to prove the estimator is reliable.

In this work, our first purpose is to construct a robust, efficient and computationally simple error estimator such that it accurately reflects the solution error distribution and achieves an optimal convergence rate. We use the PPIFE solution $u_\tau$ itself, the source term $f$, and the error equation for the PPIFE approximation to derive an estimator that contains three terms: the element residual, the numerical solution jump, and the numerical flux jump. Note that the estimator constructed here is quite different from the one in [32], which leads directly to a new analysis approach for a posterior error estimation, especially for the analysis of the elemental residual and the numerical solution jump. The second purpose of this paper is to present a new and direct approach for obtaining the reliability bounds of the estimator without involving the Helmholtz decomposition. To this end, our analysis makes full use of an $L^2$ representation of the true error and a modified Clément interpolation. Then, combined with the trace inequality for linear IFE functions, both the element residual and the numerical flux jump can be bound. We cannot, however, do the same for the numerical solution jump because the global IFE functions are discontinuous across interface edges. A special trace inequality was introduced to overcome this difficulty. On the other hand, we know that the IFE solu-

tion is a piecewise linear function on interface elements, so using the standard bubble function technique [33] to prove efficiency bounds does not apply here. We modify the standard technique according to the feature of the linear IFE basic function. However, when the interface element is irregular, the modified technique does not give explicit efficiency bounds. This bound is addressed, in this case, by an interpolation estimate in the IFE space.

The outline of this paper is as follows. The next section starts by presenting the model problem, defining some norms, and introducing the IFE space. The error equation for the PPIFE approximation is derived in Section 3, and then we construct a residual-based a posteriori error estimator. Sections 4 and 5 prove the efficiency and reliability of the residual-based a posteriori error estimator, respectively. Several numerical examples are presented in Section 6. Finally, Section 7 summarizes and proposes a further work plan.

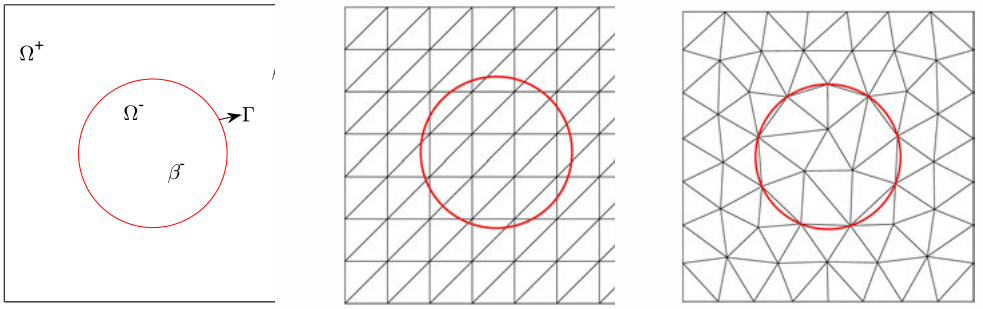


FIG. 1.1. *(a) A square domain Ω cut by an interface Γ; (b) Non-body-fitted mesh of an interface problem; (c) Body-fitted mesh of an interface problem.*

## 2. Preliminaries and partially penalized IFEM space

**2.1. Interface problem.** Let $\Omega \subset \mathbb{R}^2$ be a bounded open domain with a Lipschitz boundary $\partial\Omega$. The interface $\Gamma$ is a $C^2$-smooth curve that divides $\Omega$ into two sub-domains $\Omega^+$ and $\Omega^-$, such that $\bar{\Omega} = \overline{\Omega^+ \cap \Omega^- \cap \Gamma}$ (see Figure 1.1(a)). Further, we assume $\Gamma \cap \partial\Omega = \emptyset$. In this work, we consider the following elliptic interface problem:

$$-\nabla \cdot (\alpha \nabla u(x)) = f(x), \qquad \text{if } x \in \Omega, \tag{2.1}$$

$$u(x) = 0, \qquad \text{if } x \in \partial\Omega, \tag{2.2}$$

where $f \in L^2(\Omega)$ is a given function, the diffusion coefficient $\alpha$ is a piecewise constant function defined by

$$\alpha(x) = \begin{cases} \alpha^+, & \text{if } x \in \Omega^+, \\ \alpha^-, & \text{if } x \in \Omega^-, \end{cases}$$

and $\min\{\alpha^+, \alpha^-\} > 0$. And the exact solution $u$ satisfies jump conditions across the interface $\Gamma$:

$$[u]_\Gamma = 0 \qquad \text{and} \qquad [\alpha \nabla u \cdot \mathbf{n}]_\Gamma = 0, \tag{2.3}$$

where $\mathbf{n}$ is the unit outer normal vector of the interface $\Gamma$ with a direction that points to the domain $\Omega^+$.

In this paper, let $W_p^k(\Omega)$ be the standard Sobolev space with the standard norm $\|\cdot\|_{W_p^k(\Omega)}$ and the semi-norm $|\cdot|_{W_p^k(\Omega)}$. For any measurable open domain $B\subseteq\Omega$, we denote $B^s:=B\cap\Omega^s$, $s=\pm$. When $B^s\neq\varnothing$, $s=\pm$, we define a space as follows:

$$\widetilde{W}_p^k(B):=\left\{u\in W_p^1(B):u|_{B^s}\in W_p^k(B^s),s=+,-\right\}$$

equipped with the norm and the semi-norm

$$\|u\|_{\widetilde{W}_p^k(B)}^p=\|u\|_{W_p^k(B^+)}^p+\|u\|_{W_p^k(B^-)}^p \quad \text{and} \quad |u|_{\widetilde{W}_p^k(B)}^p=|u|_{W_p^k(B^+)}^p+|u|_{W_p^k(B^-)}^p.$$

Next, we introduce the following space:

$$PW_p^k(B)=\left\{u:u|_{B^s}\in\widetilde{W}_p^k(B^s),s=\pm;\ [u]=0,\ [\beta\nabla u\cdot\mathbf{n}_\Gamma]=0 \text{ on } \Gamma\cap B\right\}.$$

We denote $L^p(B)$ as the Lebesgue space for $1\leq p\leq\infty$, with a norm $\|\cdot\|_{L^p(B)}$. Specially, $L^2(B)$ is a Hilbert space with the inner product and norm

$$(v,w)_B=\int_B vw\,\mathrm{d}x \quad \text{and} \quad \|v\|_B=\left(\int_B|v|^2\,\mathrm{d}x\right)^{1/2}.$$

As before, $L^2(\partial B)$ is the square-integrable function space on $\partial B$ equipped with the inner product and norm

$$(v,w)_{\partial B}=\int_{\partial B}vw\,\mathrm{d}x \quad \text{and} \quad \|v\|_{\partial B}=\left(\int_{\partial B}|v|^2\,\mathrm{d}x\right)^{1/2}.$$

For $p=2$, we let $H^k(B)=W_2^k(B)$ equipped with the norm $\|\cdot\|_{H^k(B)}$ and the semi-norm $|\cdot|_{H^k(B)}$. Further, we define the Hilbert space $H_0^k(B)=\left\{v\in H^k(B):v=0 \text{ on } \partial B\right\}$. Similarly, we have $PH^k(B)=PW_2^k(B)$. If $B=\Omega$, we will omit the index $\Omega$.

The weak formulation of problems (2.1)-(2.3) then is: find $u\in H_0^1(\Omega)$ such that

$$\int_\Omega\alpha\nabla u\cdot\nabla v\,\mathrm{d}x=\int_\Omega fv\,\mathrm{d}x, \quad \text{for all } v\in H_0^1(\Omega). \tag{2.4}$$

**2.2. Partially penalized IFE space.** Let $\mathcal{T}_h=\{K\}(0<h<1)$ be a family of Cartesian triangulations of $\Omega$. Then $\mathcal{N}$, $\mathcal{E}$, and $\tilde{\mathcal{E}}$ are the corresponding sets of nodes, edges, and interior edges, respectively. Denote by $\mathcal{T}_h^{int}$ the set of interface elements in $\mathcal{T}_h$ and by $\mathcal{T}_h^{non}$ the set of non-interface elements. We assume that the interface intersects at most two edges of an interface element. If the interface intersects the element at either one vertex or two adjacent vertices, then the element is a non-interface element. This assumption is reasonable when $h$ is small enough. We denote the set of interface edges and non-interface edges of the edges $\mathcal{E}$ by $\mathcal{E}^{int}$ and $\mathcal{E}^{non}$, respectively. Similarly, we let $\tilde{\mathcal{E}}^{int}$ and $\tilde{\mathcal{E}}^{non}$ denote the set of interior interface edges and interior non-interface edges, respectively.

For any element $K\in\mathcal{T}_h$, we let $\mathcal{I}_K=\{1,2,3\}$ and $A_j,j\in\mathcal{I}_K$ denote its vertices. We define the local IFE space as follows:

$$\mathcal{S}_h(K)=\operatorname{span}\{\phi_i,i\in\mathcal{I}_K\}, \quad \text{for } K\in\mathcal{T}_h.$$

If $K \in \mathcal{T}_h^{non}$, $\phi_i, i \in \mathcal{I}_K$ are the standard linear nodal basis functions satisfying

$$\phi_i(A_j) = \begin{cases} 1, & i = j \\ 0, & i \neq j \end{cases}, \quad i, j \in \mathcal{I}_K.$$

For each $K \in \mathcal{T}_h^{int}$, we know that the two points where the interfaces $\Gamma$ and $K$ intersect do not lie on the same edge. We use $D$ and $E$ to denote the intersection of the interface and $\partial K$, and let $\bar{\mathbf{n}} = (\bar{n}_1, \bar{n}_2)$ denote the normal vector to the line segment $\overline{DE}$. The line segment partitions $K$ into two subelements, $K^+$ and $K^-$ (see Figure 2.1). Then, on the interface element $K$, the linear IFE shape functions $\phi_i, i \in \mathcal{I}_K$ are piecewise linear polynomials specified by [34, 35]:

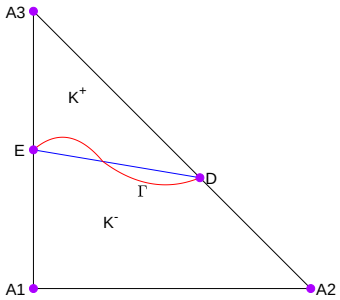


FIG. 2.1. *A triangular interface element*

$$\phi_i(x) = \begin{cases} \phi_i^+(x) = a^+ x_1 + b^+ x_2 + c^+, & \mathrm{x} \in K^+, \\ \phi_i^-(x) = a^- x_1 + b^- x_2 + c^-, & \mathrm{x} \in K^-, \end{cases} \tag{2.5}$$

where the coefficients satisfy the interface jump conditions

$$\phi_i^+(D) = \phi_i^-(D), \quad \phi_i^+(E) = \phi_i^-(E) \quad \text{and} \quad \alpha^+ \frac{\partial \phi_i^+}{\partial \bar{\mathbf{n}}} = \alpha^- \frac{\partial \phi_i^-}{\partial \bar{\mathbf{n}}}.$$

Then, we introduce the following global IFE space and piecewise linear space on $\Omega$:

$$\mathcal{S}_h(\Omega) = \left\{ v \in L^2(\Omega) : v|_K \in \mathcal{S}_h(K) \ \forall K \in \mathcal{T}_h, v \text{ is continuous at any } z \in \mathcal{N}, \text{and } v|_{\partial\Omega} = 0 \right\},$$
$$\mathcal{V}_h(\Omega) = \left\{ v : v|_K \in \mathbb{P}_1(K), \ \forall K \in \mathcal{T}_h \right\},$$

where $\mathbb{P}_1(\cdot)$ is the space of linear polynomials on element $K$.

Given $e \in \tilde{\mathcal{E}}$, we denote $K_{e,1}$ and $K_{e,2}$ as two elements that share the common edge $e$. Fix $v \in \mathcal{V}_h(\Omega)$, we define its average and jump on each edge by

$$\{v\}_e = \begin{cases} \frac{1}{2}\left(v|_{K_{e,1}} + v|_{K_{e,2}}\right), & e \in \tilde{\mathcal{E}}, \\ v|_{K_{e,1}}, & e \in \mathcal{E} \backslash \tilde{\mathcal{E}}, \end{cases} \quad \text{and} \quad [v]_e = \begin{cases} v|_{K_{e,1}} - v|_{K_{e,2}}, & e \in \tilde{\mathcal{E}}, \\ v|_{K_{e,1}}, & e \in \mathcal{E} \backslash \tilde{\mathcal{E}}. \end{cases}$$

For simplicity, we omit the subscript $e$ in these notations if there is no ambiguity.

Take any test function $v_\tau \in \mathcal{S}_h(\Omega)$ to multiply both sides of (2.1), then applying (2.2), integration by parts on each element together with the identity

$$[uv] = \{u\}[v] + [u]\{v\},$$

one obtains

$$\int_\Omega f v_\tau \,\mathrm{d}x = \sum_{K\in\mathcal{T}_h}\int_K \alpha\nabla u\cdot\nabla v\,\mathrm{d}x - \sum_{e\in\tilde{\mathcal{E}}^{int}}\int_e \{\alpha\nabla u\cdot\mathbf{n}_e\}[v_\tau]\,\mathrm{d}s. \tag{2.6}$$

Note that $[\alpha\nabla u\cdot\mathbf{n}_e]_e=0,\ \forall e\in\mathcal{E}$ and $[v_\tau]_e=0,\ \forall e\in\mathcal{E}^{non}$, where $\mathbf{n}_e$ is the unit normal vector to $e$ pointing from $K_{e,2}$ towards $K_{e,1}$. According to the regularity of $u$, for any parameter $\sigma,\epsilon>0$ and $\gamma\geq 0$, we have

$$\epsilon\sum_{e\in\tilde{\mathcal{E}}^{int}}\int_e\{\alpha\nabla v_\tau\cdot\mathbf{n}_e\}[u]\,\mathrm{d}s=0 \qquad \text{and} \qquad \sum_{e\in\tilde{\mathcal{E}}^{int}}\int_e\frac{\gamma}{|h_e|^\sigma}[u][v_\tau]\,\mathrm{d}s=0, \tag{2.7}$$

where $h_e$ denotes the length of $e$.

Inserting (2.7) into (2.6), we obtain

$$a_h(u,v_\tau)=\int_\Omega f v_\tau\,\mathrm{d}x,$$

where the bilinear form $a_h(\cdot,\cdot)$ defined by

$$\begin{aligned}a_h(u,v_\tau)=&\sum_{K\in\mathcal{T}_h}\int_K\alpha\nabla u\cdot\nabla v_\tau\,\mathrm{d}x-\sum_{e\in\tilde{\mathcal{E}}^{int}}\int_e\{\alpha\nabla u\cdot\mathbf{n}_e\}[v_\tau]\,\mathrm{d}s\\&+\epsilon\sum_{e\in\tilde{\mathcal{E}}^{int}}\int_e\{\alpha\nabla v_\tau\cdot\mathbf{n}_e\}[u]\,\mathrm{d}s+\sum_{e\in\tilde{\mathcal{E}}^{int}}\int_e\frac{\gamma}{|h_e|^\sigma}[u][v_\tau]\,\mathrm{d}s.\end{aligned}$$

We may thus formulate the following PPIFE method: find $u_\tau\in\mathcal{S}_h(\Omega)$ such that

$$a_h(u_\tau,v_\tau)=\int_\Omega f v_\tau\,\mathrm{d}x,\quad \text{for all } v_\tau\in\mathcal{S}_h(\Omega). \tag{2.8}$$

## 3. Estimator

In this section, we describe an error estimator for the PPIFE approximation. In order to estimate the true error $E=u-u_\tau$, one may make use of (i) the PPIFE solution $u_\tau$ itself, (ii) the source term $f$, and (iii) the error equation for the PPIFE approximation

$$a_h(E,v)=\int_\Omega f v\,\mathrm{d}x-a_h(u_\tau,v),\quad \text{for all } v\in H_0^1(\Omega). \tag{3.1}$$

Decompose (3.1) into local contributions from each element, to be rewritten as

$$\begin{aligned}a_h(E,v)=&\sum_{K\in\mathcal{T}_h}\int_K f v\,\mathrm{d}x-\sum_{K\in\mathcal{T}_h}\int_K\alpha\nabla u_\tau\cdot\nabla v\,\mathrm{d}x\\&-\epsilon\sum_{e\in\tilde{\mathcal{E}}^{int}}\int_e\{\alpha\nabla v\cdot\mathbf{n}_e\}[u_\tau]\,\mathrm{d}s.\end{aligned} \tag{3.2}$$

Integration by parts over each element gives

$$\sum_{K\in\mathcal{T}_h}\int_K\alpha\nabla u_\tau\cdot\nabla v\,\mathrm{d}x=-\sum_{K\in\mathcal{T}_h}\int_K\nabla\cdot(\alpha\nabla u_\tau)v\,\mathrm{d}x+\sum_{e\in\tilde{\mathcal{E}}}\int_e[\alpha\nabla u_\tau\cdot\mathbf{n_e}]\{v\}\,\mathrm{d}x. \tag{3.3}$$

Inserting (3.3) into (3.2), we get

$$a_h(E,v)=\sum_{K\in\mathcal{T}_h}\int_K R_K v\,\mathrm{d}x-\sum_{e\in\tilde{\mathcal{E}}}\int_e j_{n,e}\{v\}\,\mathrm{d}x-\epsilon\sum_{e\in\tilde{\mathcal{E}}^{int}}\int_e\{\alpha\nabla v\cdot\mathbf{n}_e\}j_{u,e}\,\mathrm{d}s, \tag{3.4}$$

where $R_K$ is the element residual

$$R_K=f+\nabla\cdot(\alpha\nabla u_\tau),\quad \text{in } K, \tag{3.5}$$

$j_{u,e}$ is the jump of the numerical solution across the edge $e$

$$j_{u,e}=[u_\tau], \tag{3.6}$$

and $j_{n,e}$ is the jump of the gradient across the edge $e$

$$j_{n,e}=[\alpha\nabla u_\tau\cdot\mathbf{n_e}]=\begin{cases}(\alpha\nabla u_\tau\cdot\mathbf{n}_e)\,|_{K_{e,1}}-(\alpha\nabla u_\tau\cdot\mathbf{n}_e)\,|_{K_{e,2}}, & \text{if } e\in\tilde{\mathcal{E}},\\ 0, & \text{if } e\in\mathcal{E}\backslash\tilde{\mathcal{E}}.\end{cases} \tag{3.7}$$

Let $\alpha_A$ and $\alpha_H$ be the arithmetic and harmonic averages of $\alpha$, defined as

$$\alpha_A=\begin{cases}\dfrac{\alpha^++\alpha^-}{2}, & x\in\Omega\backslash\partial\Omega,\\ \alpha^+, & x\in\partial\Omega,\end{cases}\quad\text{and}\quad \alpha_H=\begin{cases}\dfrac{2\alpha^+\alpha^-}{\alpha^++\alpha^-}, & x\in\Omega\backslash\partial\Omega,\\ \alpha^+, & x\in\partial\Omega.\end{cases}$$

It is easy to verify that

$$\frac{\sqrt{\alpha^+}}{2}\le\sqrt{\alpha_H},\quad \frac{\sqrt{\alpha^-}}{2}\le\sqrt{\alpha_H},\quad \frac{1}{2\sqrt{\alpha^+}}\le\frac{1}{\sqrt{\alpha_A}},\quad\text{and}\quad \frac{1}{2\sqrt{\alpha^-}}\le\frac{1}{\sqrt{\alpha_A}}. \tag{3.8}$$

The expression in (3.4) directly leads to a local error indicator $\eta_K$ defined by

$$\begin{aligned}\eta_K^2=&\sum_{e\in\mathcal{E}_K\cap\tilde{\mathcal{E}}^{int}}\left(\frac{h_e}{2\alpha_A}\|j_{n,e}\|_e^2+\frac{\alpha_H}{2h_e}\|j_{u,e}\|_e^2\right)+\frac{h_K^2}{\alpha_K}\|R_K\|_K^2\\&+\sum_{e\in\mathcal{E}_K\cap\tilde{\mathcal{E}}^{non}}\frac{h_e}{2\alpha_A}\|j_{n,e}\|_e^2,\end{aligned} \tag{3.9}$$

where $h_K$ is the diameter of $K$, $\mathcal{E}_K$ is the set of three edges of $K$, and $\alpha_K$ denotes the value of $\alpha$ restricted to $K$. Then, the global error estimator $\eta$ is defined by

$$\eta^2=\sum_{K\in\mathcal{T}_h}\eta_K^2. \tag{3.10}$$

REMARK 3.1. When $K\in\mathcal{T}_h^{non}$, the second term in (3.9) is equal to 0. Now, the error indicator only involves the element residual and the numerical flux jump. The fundamental work of efficiency bounds for both terms on non-interface elements has been established in [36,37].

## 4. Local efficiency bounds

In this section, we will establish the local efficiency bounds of the error estimator $\eta$. To this end, we first need some notations and assumptions. Given $e\in\mathcal{E}^{int}$, let $e^+=e\cap\Omega^+$ and $e^-=e\cap\Omega^-$. As before, set $K_{e^+,1}$ and $K_{e^+,2}$ as two elements that share the common edge $e^+$.

When $K\in\mathcal{T}_h^{non}$, the local indicator contains only $R_K$ and $j_{n,e}$. The efficiency bounds of both terms were addressed on non-interface elements by Verftirth [36], who used the bubble functions technique. We mainly establish here the efficiency bound of $\eta_K$ over interface elements. We know that the IFE solution is a piecewise linear function on interface elements. As a result, the technique cannot be used to prove the efficiency bound of $\eta_K$ on $K\in\mathcal{T}_h^{int}$ directly. To solve this difficulty, we define bubble functions on $K^+$ and $K^-$, respectively.

Fix a triangle element $K^+\subset K\in\mathcal{T}_h^{int}$, $\ell_i, i=1,2,3$ denote the barycentric coordinates of $K^+$. We then define the triangle-bubble function $\psi_K$ by

$$\psi_K=\begin{cases}27\ell_1\ell_2\ell_3, & \text{on } K^+,\\ 0, & \text{on } \Omega\backslash K^+.\end{cases}$$

For each $e^+\in\mathcal{E}_{K^+}\cap\mathcal{E}^{int}$, define the edge-bubble function $\psi_e$ by

$$\psi_e=\begin{cases}4\ell_1\ell_2, & \text{on } K_{e^+,1}\cup K_{e^+,2},\\ 0, & \text{on } \Omega\backslash\left(K_{e^+,1}\cup K_{e^+,2}\right).\end{cases}$$

Notice that we here let $K^+=K_{e^+,1}$. If $K^+$ is not a triangle, then it must be a quadrilateral. We divide $K^+$ into two triangles by connecting a vertex of $K^+$ and an interface intersection, e.g., connecting $D$ and $A_1$ in Figure 2.1.

The following lemma gives the bound of $R_K$ on each element $K\in\mathcal{T}_h$.

LEMMA 4.1. *Let $\bar{R}_K=\frac{1}{|K|}\int_K R_K\,\mathrm{d}x$ be the average of $R_K$ over $K\in\mathcal{T}_h$, and then the following estimate holds:*

$$\frac{h_K^2}{\alpha_K}\|R_K\|_K^2\le C\left(\left\|\alpha^{1/2}\nabla E\right\|_K^2+h_K^2\left\|\alpha^{-1/2}\left(\bar{R}_K-R_k\right)\right\|_K^2\right),\tag{4.1}$$

*where $C$ is a constant independent of the mesh size and $\alpha$.*

*Proof.* We first estimate the bound of $R_K$ on each interface element $K$. To this end, we construct an element-bubble function $\psi_K$ on $K^+$. Using the property of the element-bubble function [38], we get

$$\begin{aligned}\left\|\bar{R}_K\right\|_{K^+}^2&\le\int_{K^+}\psi_K\left(\bar{R}_K\right)^2\mathrm{d}x\\&=\int_{K^+}\nabla\cdot\left(\alpha\nabla\left(u_h-u\right)\right)\psi_K\bar{R}_K\,\mathrm{d}x+\int_{K^+}\left(\bar{R}_K-R_K\right)\psi_K\bar{R}_K\,\mathrm{d}x.\end{aligned}$$

From the definition of $\psi_K$, we can derive $\psi_K|_{\partial K^+}=0$. Furthermore, we apply Green's formula and the Cauchy-Swartz inequality to find that

$$\begin{aligned}\left\|\bar{R}_K\right\|_{K^+}^2&\le\int_{K^+}\alpha\nabla E\cdot\nabla\left(\psi_K\bar{R}_K\right)\mathrm{d}x+\int_{K^+}\left(\bar{R}_K-R_K\right)\psi_K\bar{R}_K\,\mathrm{d}x\\&\le\|\alpha\nabla E\|_{K^+}\left\|\nabla\left(\psi_K\bar{R}_K\right)\right\|_{K^+}+\left\|\bar{R}_K-R_K\right\|_{K^+}\left\|\psi_K\bar{R}_K\right\|_{K^+}.\end{aligned}$$

Noting that

$$\left\|\nabla\left(\psi_K\bar{R}_K\right)\right\|_{K^+}\le Ch_{K^+}^{-1}\left\|\bar{R}\right\|_{K^+}\quad\text{and}\quad\left\|\psi_K\bar{R}_K\right\|_{K^+}\le\left\|\bar{R}_K\right\|_{K^+}.\tag{4.2}$$

Hence, $\left\|\bar{R}_K\right\|_{K^+}$ can be bound as

$$\left\|\bar{R}_K\right\|_{K^+}\le C\left(h_{K^+}^{-1}\|\alpha\nabla E\|_{K^+}+\left\|\bar{R}_K-R_K\right\|_{K^+}\right).$$

Using the Cauchy-Swartz inequality, we arrive at

$$\|R_K\|_{K^+} \le C\left(h_{K^+}^{-1}\|\alpha\nabla E\|_{K^+} + \left\|\bar{R}_K - R_K\right\|_{K^+}\right). \tag{4.3}$$

Analogously, we construct an element-bubble function on $K^-$ to obtain

$$\|R_K\|_{K^-} \le C\left(h_{K^-}^{-1}\|\alpha\nabla E\|_{K^-} + \left\|\bar{R}_K - R_K\right\|_{K^-}\right). \tag{4.4}$$

Now, using the definition of norm, we derive

$$\begin{aligned}\frac{h_K^2}{\alpha_K}\|R_K\|_K^2 &= \frac{h_K^2}{\alpha_K}\left(\|R_K\|_{K^+}^2 + \|R_K\|_{K^-}^2\right)\\ &\le C\frac{h_K^2}{\alpha_K}\left(\max\left\{h_{K^+}^{-2}, h_{K^-}^{-2}\right\}\|\alpha\nabla E\|_K^2 + \left\|\bar{R}_K - R_K\right\|_K^2\right)\\ &\le C\left(\left\|\alpha^{1/2}\nabla E\right\|_K^2 + h_K^2\left\|\alpha^{-1/2}\left(\bar{R}_K - R_K\right)\right\|_K^2\right).\end{aligned}$$

The constant $C = Ch_K^2\max\left\{h_{K^+}^{-2}, h_{K^-}^{-2}\right\}$ in the last inequality. For $K \in \mathcal{T}_h^{non}$, we define an element-bubble function on $K$ to obtain

$$\frac{h_K^2}{\alpha_K}\|R_K\|_K^2 \le C\left(\left\|\alpha^{1/2}\nabla E\right\|_K^2 + h_K^2\left\|\alpha^{-1/2}\left(\bar{R}_K - R_K\right)\right\|_K^2\right).$$

Here the constant $C$ is independent of the interface location. This completes the proof. ∎

The estimated result of $j_{n,e}$ is stated in the lemma below.

LEMMA 4.2. *For every $e \in \tilde{\mathcal{E}}$, the following estimate holds:*

$$\frac{h_e}{2\alpha_A}\|j_{n,e}\|_e^2 \le C\left(\left\|\alpha^{1/2}\nabla E\right\|_{\omega_e}^2 + h_e^2\left\|\alpha^{-1/2}\left(\bar{R}_K - R_K\right)\right\|_{\omega_e}^2\right), \tag{4.5}$$

*where $\omega_e$ is the union of all triangles that have $e$ as an edge and the constant $C$ is independent of the mesh size and $\alpha$.*

*Proof.* We first consider an arbitrary interface edge $e \in \tilde{\mathcal{E}}^{int}$. Denote by $\psi_e$ the edge-bubble function on $e^+$. We can deduce from the properties of $\psi_e$ and the continuity of $\alpha\nabla u\cdot\mathbf{n}$ that

$$\|j_{n,e}\|_{e^+}^2 \le \int_{e^+}[\alpha\nabla u_\tau\cdot\mathbf{n}_e]\psi_e j_{n,e}\,\mathrm{d}x \le \int_{e^+}[\alpha\nabla(u_\tau - u)\cdot\mathbf{n}_e]\psi_e j_{n,e}\,\mathrm{d}x.$$

Noting that $\psi_e$ is equal to zeros on $\partial\omega_{e^+}$. Next, applying Green's formula gives

$$\int_{e^+}(\alpha\nabla(u_\tau - u)\cdot\mathbf{n}_e)|_{K_{e,1}}\psi_e j_{n,e}\,\mathrm{d}x = \int_{K_{e^+,1}} R_K\psi_e j_{n,e} + \alpha\nabla(u_\tau - u)\cdot\nabla(\psi_e j_{n,e})\,\mathrm{d}x.$$

Hence, we have

$$\|j_{n,e}\|_{e^+}^2 \le \int_{\omega_{e^+}} R_K\psi_e j_{n,e} + \alpha\nabla(u_\tau - u)\cdot\nabla(\psi_e j_{n,e})\,\mathrm{d}x.$$

From the properties of $\psi_e$ [38], on the other hand, we know that

$$\|\nabla(\psi_e j_{n,e})\|_{\omega_{e^+}} \le Ch_{e^+}^{-1/2}\|j_{n,e}\|_{e^+} \quad \text{and} \quad \|\psi_e j_{n,e}\|_{\omega_{e^+}} \le Ch_{e^+}^{1/2}\|j_{n,e}\|_{e^+}. \tag{4.6}$$

Using the Cauchy-Schwarz inequality and (4.6) yields the error estimate

$$\|j_{n,e}\|_{e^+} \le C\left(h_{e^+}^{-1/2}\|\alpha\nabla E\|_{\omega_{e^+}} + h_{e^+}^{1/2}\|R_K\|_{\omega_{e^+}}\right). \tag{4.7}$$

Afterward, we apply (4.3) and (3.8) to obtain

$$\|j_{n,e}\|_{e^+} \le C\left(h_{e^+}^{-1/2}\|\alpha\nabla E\|_{\omega_{e^+}} + h_e^{1/2}\left\|\bar{R}_K - R_K\right\|_{\omega_{e^+}}\right). \tag{4.8}$$

Similarly, we define $\psi_e$ on $e^-$ to get

$$\|j_{n,e}\|_{e^-} \le C\left(h_{e^-}^{-1/2}\|\alpha\nabla E\|_{\omega_{e^-}} + h_e^{1/2}\left\|\bar{R}_K - R_K\right\|_{\omega_{e^-}}\right). \tag{4.9}$$

This and (4.8) imply

$$\begin{aligned} h_e\|j_{n,e}\|_e^2 &= h_e\left(\|j_{n,e}\|_{e^+}^2 + \|j_{n,e}\|_{e^-}^2\right) \\ &\le Ch_e\left(\max\left\{h_{e^+}^{-1}, h_{e^-}^{-1}\right\}\|\alpha\nabla E\|_{\omega_e}^2 + h_e\left\|\bar{R}_K - R_K\right\|_{\omega_e}^2\right) \\ &\le C\alpha_A\left(\left\|\alpha^{1/2}\nabla E\right\|_{\omega_e}^2 + h_e^2\left\|\alpha^{-1/2}\left(\bar{R}_K - R_K\right)\right\|_{\omega_e}^2\right). \end{aligned}$$

The constant $C = Ch_e\max\left\{h_{e^+}^{-1}, h_{e^-}^{-1}\right\}$ in the last inequality. For each non-interface edge $e \in \tilde{\mathcal{E}}^{non}$, we define an edge-bubble function on $e$ to obtain

$$\frac{h_e}{\alpha_A}\|j_{n,e}\|_e^2 \le C\left(\left\|\alpha^{1/2}\nabla E\right\|_{\omega_e}^2 + h_e^2\left\|\alpha^{-1/2}\left(\bar{R}_K - R_K\right)\right\|_{\omega_e}^2\right). \tag{4.10}$$

The constant $C$ is independent of the interface location. This completes the proof. ∎

With a similar argument in Lemma 4.2, we can give the estimate of $j_{u,e}$.

LEMMA 4.3. *There is a constant $C$ such that, on each interface edge $e \in \tilde{\mathcal{E}}^{int}$, the following estimate holds:*

$$\frac{\alpha_H}{2h_e}\|j_{u,e}\|_e^2 \le C\left\|\alpha^{1/2}\nabla E\right\|_{\omega_e}^2. \tag{4.11}$$

*The constant $C$ is independent of the mesh size and $\alpha$.*

*Proof.* For an interior edge $e \in \tilde{\mathcal{E}}$, the unit normal and tangential vectors to $e$ are denoted by $\mathbf{n}_e = (x_e, y_e)$ and $\mathbf{t}_e = (-y_e, x_e)$, respectively. Given $v \in H_0^1(\Omega)$, define $j_{t,e} = [\nabla u \cdot \mathbf{t}_e]_e$ as the tangential derivative jump across the edge $e$ and $\nabla^\perp v = \left(\dfrac{\partial v}{\partial y}, -\dfrac{\partial v}{\partial x}\right)$ as the formal adjoint operator of the curl operator. Our goal here is to prove the efficiency bound of $\|j_{u,e}\|_e$. From [32], however, we know that

$$\|j_{u,e}\|_{e^+} \le Ch_{e^+}\|j_{t,e}\|_{e^+}. \tag{4.12}$$

Next, we adopt the same method as in Lemma 4.2 to give the efficiency bound of $\|j_{t,e}\|_{e^+}$. For each interface edge $e \in \tilde{\mathcal{E}}^{int}$, we define an edge-bubble function $\psi_e$ on $e^+$. Applying the properties of $\psi_e$, the continuity of $\nabla u \cdot \mathbf{t}_e$ and Green's formula to deduce that

$$\begin{aligned} \|j_{t,e}\|_{e^+}^2 &\le C\int_{e^+}[\nabla u_\tau \cdot \mathbf{t}_e]\, j_{t,e}\psi_e\,\mathrm{d}x \le C\int_{\omega_{e^+}}\nabla(u_\tau - u)\cdot\nabla^\perp(j_{t,e}\psi_e)\,\mathrm{d}x \\ &\le C\|\nabla E\|_{\omega_{e^+}}\|\nabla(j_{t,e}\psi_e)\|_{\omega_{e^+}}. \end{aligned}$$

Similar to (4.6), we have

$$\|\nabla(j_{t,e}\psi_e)\|_{\omega_{e^+}} \leq Ch_{e^+}^{-1/2}\|j_{t,e}\|_{e^+}.$$

Hence, one obtains

$$\|j_{t,e}\|_{e^+} \leq Ch_{e^+}^{-1/2}\|\alpha\nabla E\|_{\omega_{e^+}}. \tag{4.13}$$

Applying (4.12), it is derived that

$$\|j_{u,e}\|_{e^+} \leq Ch_e^{1/2}\|\alpha\nabla E\|_{\omega_{e^+}}. \tag{4.14}$$

Analogously, we get

$$\|j_{u,e}\|_{e^-} \leq Ch_e^{1/2}\|\alpha\nabla E\|_{\omega_{e^-}}. \tag{4.15}$$

Using the definition of norm and (3.8) yields

$$h_e^{-1}\|j_{u,e}\|_e^2 = h_e^{-1}\left(\|j_{u,e}\|_{e^+}^2 + \|j_{u,e}\|_{e^-}^2\right) \leq C\alpha_H^{-1}\left\|\alpha^{1/2}\nabla E\right\|_{\omega_e}^2,$$

which completes our proof. ∎

The following theorem is a direct consequence of the above three lemmas.

THEOREM 4.1. *Let $u \in PH^2(\Omega)\cap H_0^1(\Omega)$ and $u_\tau$ be the unique solution of problems (2.4) and (2.8), respectively. Then, there exists a constant $C$ independent of the mesh size and $\alpha$, such that*

$$\eta_K \leq C\left(\left\|\alpha^{1/2}\nabla E\right\|_{\omega_K} + h_K\left\|\alpha^{-1/2}\left(\bar{R}_K - R_K\right)\right\|_{\omega_K}\right), \tag{4.16}$$

*where $\omega_K$ denotes the set of all elements $\hat{K} \in \mathcal{T}_h$ that share an edge with $K$.*

REMARK 4.1. The constant $C$ in Lemma 4.1 and Lemma 4.2 depends on $\max\{h_{e^+}^{-1}, h_{e^-}^{-1}\}$. If the intersection of the interface and an interface edge and the element vertexes are infinitely close, the constant $C$ makes no sense. In this case, the interface element can be approximated as a non-interface element. It implies that there may exist a constant controlling the efficiency bound. The following lemma proves our conjecture.

LEMMA 4.4. *There exist constants $C_i > 0, i = 1,2,3$, for each $K \in \mathcal{T}_h$, such that*

$$\frac{h_K}{\sqrt{\alpha_K}}\|R_K\|_K \leq C_1\left(\left\|\alpha^{1/2}\nabla E\right\|_K + h_K\left\|\alpha^{-1/2}\left(\bar{R}_K - R_K\right)\right\|_K + h_K\min\{h_{e^+}, h_{e^-}\}\right), \tag{4.17}$$

$$\sqrt{\frac{\alpha_H}{2h_e}}\|j_{u,e}\|_e \leq C_2\left(\left\|\alpha^{1/2}\nabla E\right\|_{\omega_e} + h_e\min\left\{\sqrt{h_{e^-}}, \sqrt{h_{e^+}}\right\}\right), \quad e \in \mathcal{E}_K \cap \tilde{\mathcal{E}}^{int}, \tag{4.18}$$

$$\sqrt{\frac{h_e}{2\alpha_A}}\|j_{n,e}\|_e \leq C_3\left(\left\|\alpha^{\frac{1}{2}}\nabla E\right\|_{\omega_e} + h_K\left\|\alpha^{-\frac{1}{2}}\left(\bar{R}_K - R_K\right)\right\|_{\omega_e} + h_e\min\left\{\sqrt{h_{e^-}}, \sqrt{h_{e^+}}\right\}\right), \tag{4.19}$$

*where $e \in \mathcal{E}_K \cap \tilde{\mathcal{E}}$ in the third inequality, and the contants $C_i\,(i = 1,2,3)$ are independent of the mesh size and $\alpha$.*

*Proof.* Without loss of generality, we assume that $h_{e^+} \gg h_{e^-}$. By the Cauchy inequality, we then have

$$\|R_K\|_K = \left(\|R_K\|_{K^+}^2 + \|R_K\|_{K^-}^2\right)^{1/2} \leq C\left(\|R_K\|_{K^+} + \|R_K\|_{K^-}\right). \tag{4.20}$$

To the first term on the right-hand side of (4.20), applying the standard efficiency bound result in Lemma 4.1, we arrive at

$$\frac{h_K}{\sqrt{\alpha_K}}\|R_K\|_{K^+} \leq C\left(\left\|\alpha^{1/2}\nabla E\right\|_K + h_K\left\|\alpha^{-1/2}\left(\bar{R}_K - R_K\right)\right\|_K\right). \tag{4.21}$$

We define an interpolation operator $P_h$: $PH^2(\Omega)\cap H_0^1(\Omega) \to \mathcal{S}_h(\Omega)$. The second term on the right-hand side of (4.20) follows from the Cauchy-Schwarz inequality and Green's formula such that

$$\begin{aligned}
\|R_K\|_{K^-} &\leq h_{K^-}^{-1}\left\|\bar{R}_K + \nabla\cdot(\alpha\nabla u_\tau)\right\|_{L^1(K^-)} + \left\|f - \bar{R}_K\right\|_{K^-} \\
&\leq h_{K^-}^{-1}\left\|f + \nabla\cdot(\alpha\nabla u_\tau)\right\|_{L^1(K^-)} + h_{K^-}^{-1}\left\|f - \bar{R}_K\right\|_{L^1(K^-)} + \left\|f - \bar{R}_K\right\|_{K^-} \\
&\leq h_{K^-}^{-1}\left\|\alpha\nabla(u_\tau - P_h u)\cdot\mathbf{n}\right\|_{L^1(\partial K^-)} + h_{K^-}^{-1}\left\|\alpha\nabla(u - P_h u)\cdot\mathbf{n}\right\|_{L^1(\partial K^-)} \\
&\quad + h_{K^-}^{-1}\left\|f - \bar{R}_K\right\|_{L^1(K^-)} + \left\|f - \bar{R}_K\right\|_{K^-}.
\end{aligned}$$

Applying the Hölder inequality, we have

$$\left\|\alpha\nabla(u_\tau - P_h u)\cdot\mathbf{n}_e\right\|_{L^1(e)} \leq h_e^{1/2}\left\|\alpha\nabla(u_\tau - u)\cdot\mathbf{n}_e\right\|_e, \quad e\in\partial K^-, \tag{4.22}$$

and

$$\left\|f - \bar{R}_K\right\|_{L^1(K^-)} \leq h_{K^-}\left\|f - \bar{R}_K\right\|_{K^-}. \tag{4.23}$$

Now, a direct application of (4.22) and (4.23) gives

$$\|R_K\|_{K^-} \leq h_{K^-}^{-\frac{1}{2}}\left\|\alpha\nabla(u_\tau - P_h u)\cdot\mathbf{n}\right\|_{\partial K^-} + h_{K^-}^{-\frac{1}{2}}\left\|\alpha\nabla(u - P_h u)\cdot\mathbf{n}\right\|_{\partial K^-} + \left\|R_K - \bar{R}_K\right\|_{K^-}. \tag{4.24}$$

The first term in (4.24) enjoys the following estimate [32]:

$$h_{K^-}^{-1/2}\left\|\alpha\nabla(u_\tau - P_h u)\cdot\mathbf{n}\right\|_{\partial K^-} \leq C\sqrt{\alpha^-}. \tag{4.25}$$

From [24], we know that the interpolation $P_h u$ in the IFE space $\mathcal{S}_h(\Omega)$ satisfies the estimate

$$\left\|\alpha\nabla(u - P_h u)|_K\cdot\mathbf{n}_e\right\|_e^2 \leq Ch^3\|u\|_{PW_\infty^2(\Omega)}^2, \quad \forall e\in\mathcal{E}^{int}.$$

Using this estimate yields

$$h_{K^-}^{-1/2}\left\|\alpha\nabla(u - P_h u)\cdot\mathbf{n}\right\|_{\partial K^-} \leq Ch_{K^-}. \tag{4.26}$$

Hence, utilizing (4.25) and (4.26), we get

$$\frac{h_K}{\sqrt{\alpha_K}}\|R_K\|_{K^-} \leq C\left(h_K + h_K h_{K^-} + h_K\left\|\alpha^{-1/2}\left(R_K - \bar{R}_K\right)\right\|_{K^-}\right).$$

Finally, combining this bound with (4.21) yields (4.17). And from Lemma 5.2 in [32] and (3.8), we directly obtain (4.18) and (4.19) to complete the proof of the lemma. ∎

## 5. Global reliability bound

In this section, we shall prove the global reliability bound of the estimator. To this end, we need to introduce an $L^2$ representation of the true error, the trace inequality for linear IFE functions, and a modified Clément interpolation operator.

Given $z\in\mathcal{N}$ set

$$\pi_z v=\begin{cases}\dfrac{\int_{\omega_z} v\phi_z\,\mathrm{d}x}{\int_{\omega_z}\phi_z\,\mathrm{d}x}, & \forall z\in\tilde{\mathcal{N}},\\ 0, & \forall z\in\mathcal{N}\backslash\tilde{\mathcal{N}},\end{cases}\tag{5.1}$$

where $\phi_z\in\mathcal{S}_h(\Omega)$ is the linear IFE nodal basis function at $z\in\mathcal{N}$, $\omega_z$ is the union of all triangles that have $z$ as a vertex, and $\tilde{\mathcal{N}}$ denotes the set of all vertices in $\mathcal{N}$ except those on $\partial\Omega$. We define a modified Clément interpolation operator $\mathcal{I}_h: H_0^1(\Omega)\to\mathcal{S}_h(\Omega)$ by

$$\mathcal{I}_h v=\sum_{z\in\mathcal{N}}(\pi_z v)\phi_z.\tag{5.2}$$

We recall the following modified Clément interpolation estimates, which are proved in Lemma 4.3 in [32].

LEMMA 5.1. *For each $v\in H_0^1(\Omega)$, let $\mathcal{I}_h v\in\mathcal{S}_h(\Omega)$ be a modified Clément interpolation of $v$. There exists a constant $C$ independent of the mesh size and the interface location, such that*

$$\|v-\mathcal{I}_h v\|_K\le Ch_K\|\nabla v\|_{\omega_K},\qquad \forall K\in\mathcal{T}_h,\tag{5.3}$$

$$\|\nabla(v-\mathcal{I}_h v)\|_K\le C\|\nabla v\|_{\omega_K},\qquad \forall K\in\mathcal{T}_h,\tag{5.4}$$

$$\|(v-\mathcal{I}_h v)|_K\|_e\le Ch_e^{1/2}\|\nabla v\|_{\omega_K},\qquad \forall e\in\mathcal{E}_K \text{ and } K\in\{K_{e,1},K_{e,2}\}.\tag{5.5}$$

REMARK 5.1. The interpolation operator $\mathcal{I}_h v$ we define here is slightly different from that in [32]. In this work, $\pi_z v$ only involves the linear IFE nodal basis function. However, $\pi_z v$ in this literature [32] involves both the classical barycentric hat function and the linear IFE nodal basis function. It is verified that the operator $\mathcal{I}_h v$ defined in (5.2) also satisfies the above interpolation estimate.

The trace inequality for linear IFE functions is stated in the following lemma.

LEMMA 5.2. *For each $v\in\mathcal{S}_h(\Omega)$ on $K\in\mathcal{T}_h^{int}$, the following inequality holds:*

$$\|\beta\nabla v\cdot\mathbf{n}_e\|_e\le Ch_K^{-1/2}\|\beta\nabla v\|_K,\tag{5.6}$$

*where $C$ is a constant independent of the interface location and the mesh size.*

The following lemma gives an $L^2$ representation of the true error, which is one of the key points in our error analysis.

LEMMA 5.3. *We have the following $L^2$ representation of the true error $E$:*

$$\begin{aligned}\left\|\alpha^{1/2}\nabla E\right\|_\Omega^2=&\sum_{K\in\mathcal{T}_h}\int_K R_K(E-E_h)\,\mathrm{d}x+\sum_{e\in\tilde{\mathcal{E}}}\int_e j_{n,e}\{E-E_h\}\,\mathrm{d}s\\&-\sum_{e\in\tilde{\mathcal{E}}^{int}}\int_e\{\alpha\nabla E\cdot\mathbf{n}_e\}j_{u,e}\,\mathrm{d}s+\epsilon\sum_{e\in\tilde{\mathcal{E}}^{int}}\int_e\{\alpha\nabla E_h\cdot\mathbf{n}_e\}j_{u,e}\,\mathrm{d}s+\sum_{e\in\tilde{\mathcal{E}}^{int}}\int_e\frac{\gamma}{|h_e|^\sigma}j_{u,e}[E_h]\,\mathrm{d}s,\end{aligned}\tag{5.7}$$

*where set* $E_h = \mathcal{I}_h E$.

*Proof.* According to the definition of the $L^2$ norm, we have

$$\left\|\alpha^{1/2}\nabla E\right\|_\Omega^2 = (\alpha\nabla E, \nabla E) = (\alpha\nabla E, \nabla(E-E_h)) + (\alpha\nabla E, \nabla E_h).$$

Since $a_h(u_\tau, v_\tau) = (f, v_\tau)$ and $a_h(u, v_\tau) = (f, v_\tau)$ for all $v_\tau \in \mathcal{S}_h(\Omega)$, we have $a_h(u-u_\tau, v_\tau) = 0$. Choosing $v_\tau = E_h$, we get

$$\begin{aligned}(\alpha\nabla E, \nabla E_h) = &\sum_{e\in\tilde{\mathcal{E}}^{int}} \int_e \{\alpha\nabla E\cdot\mathbf{n}_e\}[E_h]\,\mathrm{d}s + \epsilon \sum_{e\in\tilde{\mathcal{E}}^{int}} \int_e \{\alpha\nabla E_h\cdot\mathbf{n}_e\}[u_\tau]\,\mathrm{d}s \\ &+ \sum_{e\in\tilde{\mathcal{E}}^{int}} \int_e \frac{\gamma}{|h_e|^\sigma}[u_\tau][E_h]\,\mathrm{d}s. \end{aligned} \tag{5.8}$$

Integration by parts elementwise and the observation that $E - E_h$ vanishes on $\partial\Omega$ yields

$$\begin{aligned}(\alpha\nabla E, \nabla(E-E_h)) &= \sum_{K\in\mathcal{T}_h} \int_K \alpha\nabla E\cdot\nabla(E-E_h)\,\mathrm{d}x \\ &= \sum_{K\in\mathcal{T}_h} \int_K R_K(E-E_h)\,\mathrm{d}x + \sum_{e\in\tilde{\mathcal{E}}} \int_e j_{n,e}\{E-E_h\}\,\mathrm{d}s \\ &\quad + \sum_{e\in\tilde{\mathcal{E}}^{int}} \int_e \{\alpha\nabla E\cdot\mathbf{n}_e\}\ [E-E_h]\,\mathrm{d}s. \end{aligned} \tag{5.9}$$

Together with Equation (5.8), we directly obtain this result (5.7) to complete the proof of the lemma. ∎

Below, we establish a reliability bound of the estimator.

THEOREM 5.1. *Let* $u \in PH^2(\Omega)\cap H_0^1(\Omega)$ *and* $u_\tau$ *represent the solutions to the problems* (2.4) *and* (2.8)*, respectively. There exits a constant* $C$ *independent of the interface location and the mesh size, such that*

$$\|\alpha^{1/2}\nabla E\| \le C\eta. \tag{5.10}$$

*Proof.* Every term in the $L^2$ representation of $E$ in Lemma 5.3 is denoted by $I_i$ $(i = 1,2,\ldots,5)$

$$\|\alpha^{1/2}\nabla E\|^2 := I_1 + I_2 + I_3 + I_4 + I_5. \tag{5.11}$$

Applying the Cauchy inequality to the first term in (5.11) leads to

$$I_1 \le \left(\sum_{K\in\mathcal{T}_h} \frac{(h_K)^2}{\alpha_K}\|R_K\|_K^2\right)^{1/2} \left(\sum_{K\in\mathcal{T}_h} \frac{\alpha_K}{(h_K)^2}\|E-E_h\|_K^2\right)^{1/2}.$$

From the results of Lemma 5.1, we then conclude that

$$\frac{1}{(h_K)^2}\left\|\alpha^{1/2}(E-E_h)\right\|_K^2 \le C\left\|\alpha^{1/2}\nabla E\right\|_{\omega_K}^2, \quad \text{for all } K\in\mathcal{T}_h.$$

Hence, we get

$$I_1 \le C\left\|\alpha^{1/2}\nabla E\right\| \left(\sum_{K\in\mathcal{T}_h} \frac{(h_K)^2}{\alpha_K}\|R_K\|_K^2\right)^{1/2}. \tag{5.12}$$

To bound $I_2$, from the Cauchy-Schwarz inequality, we arrive at

$$\begin{aligned} I_2 &\le \sum_{e\in\tilde{\mathcal{E}}} \|j_{n,e}\|_e \left( \frac{1}{2} \left\| (E-E_h)|_{K_{e,1}} \right\|_e + \frac{1}{2} \left\| (E-E_h)|_{k_{e,2}} \right\|_e \right) \\ &\le \left( \sum_{e\in\tilde{\mathcal{E}}} h_e \|j_{n,e}\|_e^2 \right)^{1/2} \left( \sum_{i=1,2} \left( \sum_{e\in\tilde{\mathcal{E}}} \frac{1}{4h_e} \left\| (E-E_h)|_{K_{e,i}} \right\|_e^2 \right)^{1/2} \right). \end{aligned}$$

Further, we use (3.8) and (5.5) to obtain

$$\frac{1}{4h_e} \|E-E_h\|_e^2 \le \frac{1}{\alpha_A} \left\| \alpha^{1/2} \nabla E \right\|_{\omega_e}^2. \tag{5.13}$$

Then, we have

$$I_2 \le C \left\| \alpha^{1/2} \nabla E \right\| \left( \sum_{e\in\tilde{\mathcal{E}}} \frac{h_e}{\alpha_A} \|j_{n,e}\|_e^2 \right)^{1/2}. \tag{5.14}$$

For any $v \in H^{1+s}(K)(s>0)$ with $\Delta v \in L^2(K)$, and the following inequality holds [39]

$$\int_e (\nabla v \cdot \mathbf{n}_e) w_h \, \mathrm{d}s \le C h_e^{-1/2} \|w_h\|_e \left( \|\nabla v\|_K + h_K \|\Delta v\|_K \right), \quad w_h \in \mathbb{P}_1(K). \tag{5.15}$$

Applying this estimate, (3.8) and the bound of $R_K$ yields

$$\begin{aligned} I_3 &\le C \sum_{e\in\tilde{\mathcal{E}}^{int}} h_e^{-1/2} \|j_{u,e}\|_e \left( \sum_{K\in\omega_e} \|\alpha \nabla E\|_K + h_K \|R_K\|_K \right) \\ &\le C \left( \left\| \alpha^{1/2} \nabla E \right\| + \sum_{K\in\mathcal{T}_K} h_K \left\| \alpha^{-1/2} \left( \bar{R}_K - R_K \right) \right\|_K \right) \sum_{e\in\tilde{\mathcal{E}}^{int}} \sqrt{\frac{\alpha_H}{h_e}} \|j_{u,e}\|_e. \end{aligned}$$

To bound the fourth term in (5.11), the key is the trace inequality in Lemma 5.2, which together with (3.8) and (5.4), yields

$$\begin{aligned} I_4 &\le C \sum_{e\in\tilde{\mathcal{E}}^{int}} \|j_{u,e}\|_e \left( \sum_{K\in\omega_e} h_e^{-1/2} \|\alpha \nabla E_h\|_K \right) \\ &\le C \sum_{e\in\tilde{\mathcal{E}}^{int}} \|j_{u,e}\|_e \left( \sum_{K\in\omega_e} h_e^{-1/2} \|\alpha \nabla (E_h - E)\|_K + h_e^{-1/2} \|\alpha \nabla E\|_K \right) \\ &\le C \|\alpha \nabla E\| \sum_{e\in\tilde{\mathcal{E}}^{int}} \sqrt{\frac{\alpha_H}{h_e}} \|j_{u,e}\|_e. \end{aligned}$$

To bound $I_5$, by the Cauchy-Schwarz inequality and the inverse inequality, we get

$$I_5 \le C \sum_{e\in\tilde{\mathcal{E}}^{int}} \|j_{u,e}\|_e \|[E_h]\|_e \le C \sum_{e\in\tilde{\mathcal{E}}^{int}} h_e^{-1/2} \|j_{u,e}\|_e \|E_h\|_{\omega_e}.$$

Further, the function $E_h$ in space $\mathcal{S}_h(\Omega)$ is characterized by the property $E_h|_{\partial\Omega}=0$. By the Poincaré inequality and (5.4), we have

$$\|E_h\|_\Omega \le C\|\nabla E_h\|_\Omega \le C\sum_{K\in\mathcal{T}_h}\|\nabla E\|_K + \|\nabla(E-E_h)\|_K \le C\sum_{K\in\mathcal{T}_h}\|\nabla E\|_K. \tag{5.16}$$

Hence, by (3.8), it follows that

$$I_5 \le C\left\|\alpha^{1/2}\nabla E\right\|\sum_{e\in\tilde{\mathcal{E}}^{int}}\sqrt{\frac{\alpha_H}{h_e}}\|j_{u,e}\|_e.$$

Finally, these estimates, together with Young's inequality and the definition of $\eta$, eventually prove the theorem. ∎

## 6. Numerical examples

In this section, we present several numerical experiments to verify the efficiency and reliability of the a posteriori error estimator. Besides, we propose a corresponding adaptive refinement strategy and apply it to all kinds of test problems. The standard adaptive refinement process is depicted as follows:

**Solve** → **Estimate** → **Remark** → **Refine**.

In our numerical experiments, the adaptive refinement strategy is performed specifically as follows:

(1) Solve PPIFE numerical solution $u_\tau^{(i)}$ on a given polygonal mesh $\mathcal{T}_h^i$,

(2) Estimate the error indicator $\eta_K^i$ for each element defined in (3.1),

(3) Mark the elements to be refined, and then select into a "marked" set $\widehat{\mathcal{T}}_h^i$ such that, for a given parameter $\vartheta=0.5$,

$$\sum_{\widehat{K}\in\widehat{\mathcal{T}}_h^i}\eta_{\widehat{K}}^2 \ge \vartheta\sum_{K\in\mathcal{T}_h^i}\eta_K^2,$$

(4) Refine each element $\widehat{K}\in\widehat{\mathcal{T}}_h^i$ to get a new mesh $\mathcal{T}_h^{i+1}$,

(5) Repeat steps (1)-(4) until the preset conditions are met.

Our main goal is to test the performance of the estimator and the corresponding adaptive refinement strategy for different jump ratios or interface geometries. For the goal, we will first consider solving the dual thermal conductivity problem [24, 40] with a circular interface at different jump ratios. We then chose an interface problem with a flower-like interface [41] to test the applicability of the estimator at a moderate jump ratio. We refer to the MATLAB-based finite element package iFEM [42] for the simulations.

**6.1. Example 1.** A circular interface $\Gamma$ divides the domain $\Omega=[-1,1]\times[-1,1]$ into separate regions

$$\Omega^+=\left\{(x_1,x_2):\sqrt{x_1^2+x_2^2}>r_0\right\} \quad \text{and} \quad \Omega^-=\left\{(x_1,x_2):\sqrt{x_1^2+x_2^2}\le r_0\right\},$$

where $r_0=\pi/6.28$. The solution of (2.1)-(2.3) is given by

$$u(x)=\begin{cases}\dfrac{1}{\beta^-}\left(x_1^2+x_2^2\right)^{3/2}, & \text{if } (x_1,x_2)\in\Omega^-,\\[2ex] \dfrac{1}{\beta^+}\left(x_1^2+x_2^2\right)^{3/2}+\left(\dfrac{1}{\beta^-}-\dfrac{1}{\beta^+}\right)r_0^3, & \text{if } (x_1,x_2)\in\Omega^+.\end{cases}$$

The source term $f$ is as follows:

$$f = -25\left(x_1^2 + x_2^2\right)^{3/2}.$$

We test the performance of the estimator by comparing the convergence errors obtained on a sequence of meshes that are either uniformly or adaptively refined starting from a given $8\times 8$ Cartesian triangular initial mesh. We solve the above problem for two typical different jump ratios: $\beta^+/\beta^- = 100$ (moderate jump) and $\beta^+/\beta^- = 10^4$ (large jump). Figure 6.1 reports the estimated error and the error $\left\|\alpha^{1/2}\nabla(u-u_\tau)\right\|$ on uniformly and adaptively refined meshes for the case of the two typical different jump ratios. As can be seen, the error and the estimator curves on the uniform and adaptive meshes are parallel to $N^{-1/2}$, where $N$ is the total number of degrees of freedom. Moreover, all the errors converge toward zero as $h = \max_{K\in\mathcal{T}_h}\{h_K\}$ vanishes, and they behave identically whatever the jump ratios are. However, in the same case, the errors are smaller and decrease much faster on adaptive meshes. On the other hand, we observed that the estimator gives an upper bound on the error, as predicted by the theory. Based on these results, we can conclude that the estimator and the error $\left\|\alpha^{1/2}\nabla(u-u_\tau)\right\|$ distribution match quite well for both the jump ratios.

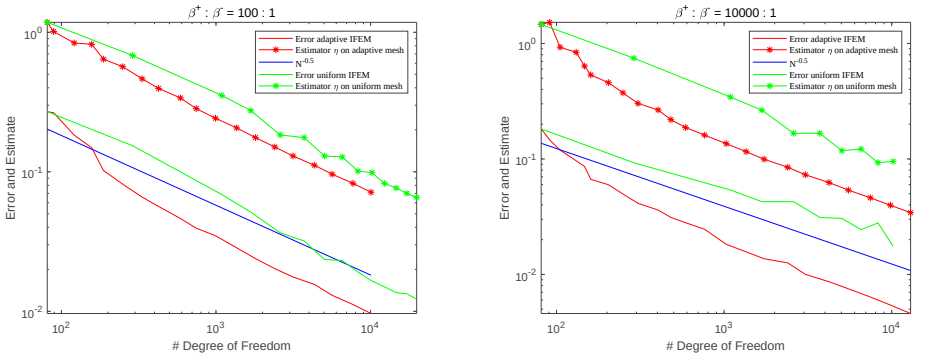


(a) (b)

FIG. 6.1. *Convergence of the error and the estimator on uniformly and adaptively refined meshes.*

The adaptively generated triangulations for both different jump ratios are visualized in Figure 6.2. Note that the adaptive meshes in the two typical jump ratios are slightly different. Here we see that the refinement is concentrated only near the interface for $\beta^+/\beta^- = 10^4$. In comparison, for $\beta^+/\beta^- = 100$, there is a part of the refinement that is near the boundary. We know that the IFE methods usually have a larger error over interface elements. When $\beta^+/\beta^- = 100$, however, we observe that the error is larger over both interface elements and boundary elements. Therefore, there is one slight difference. This shows that the error indicator precisely detects these errors, and the adaptive algorithm refines accordingly. From Figures 6.3 and 6.4, we can easily see that the adaptive refinement significantly reduces pointwise errors in the vicinity of the interface.

**6.2. Example 2.** To test the applicability of our estimator, we consider here a flower-like interface, as illustrated in Figure 6.5(a). In this example, we tested on the

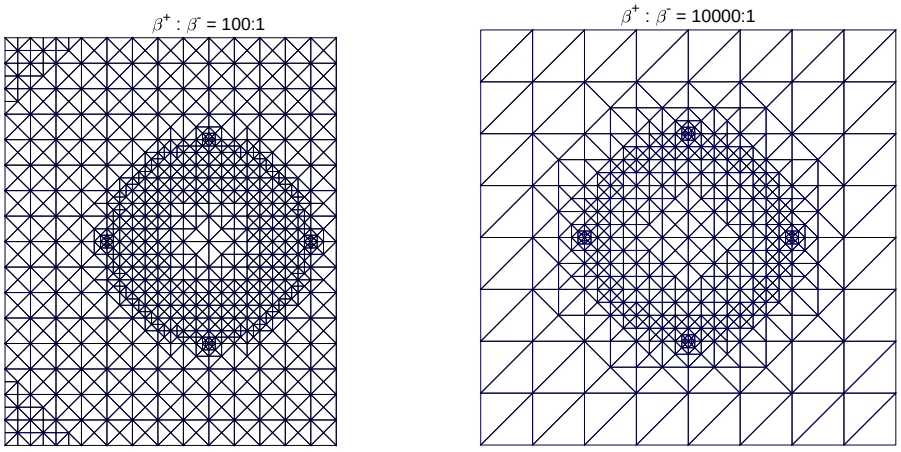


(a) 10th iterations with 1896 tri

(b) 10th iterations with 928 triangles.

FIG. 6.2. *Adaptive meshes*

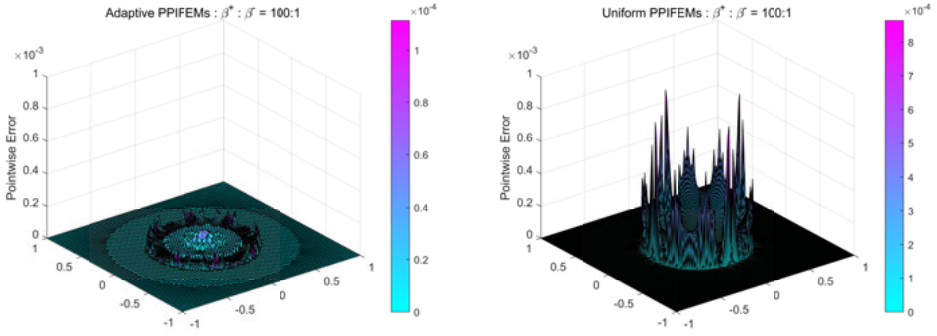


(a) Adaptive meshes

(b) Uniform meshes

FIG. 6.3. *The pointwise errors on uniformly and adaptively refined meshes for* $\beta^+/\beta^- = 100$.

same domain as in Example 6.1. The exact solution is given by

$$u = \begin{cases} \dfrac{\left(x_1^2+x_2^2\right)^2\left(1+0.4\sin\left(6\arctan\left(x_2/x_1\right)\right)\right)-0.3}{\beta^-}, & \text{if } (x_1,x_2)\in\Omega^-, \\ \dfrac{\left(x_1^2+x_2^2\right)^2\left(1+0.4\sin\left(6\arctan\left(x_2/x_1\right)\right)\right)-0.3}{\beta^+}, & \text{if } (x_1,x_2)\in\Omega^+. \end{cases}$$

For initial meshes, we use a $16\times 16$ Cartesian triangular mesh. To compare the performance of the estimator in different interface geometries, we chose a moderate jump of $\beta^+ = 100$ and $\beta^- = 1$. The adaptively generated triangulations at levels four, eight, and twelve are depicted in Figures 6.5(b)-6.5(d). We observe that the adaptive process correctly refines the triangles in the regions of the interface and boundary, as in

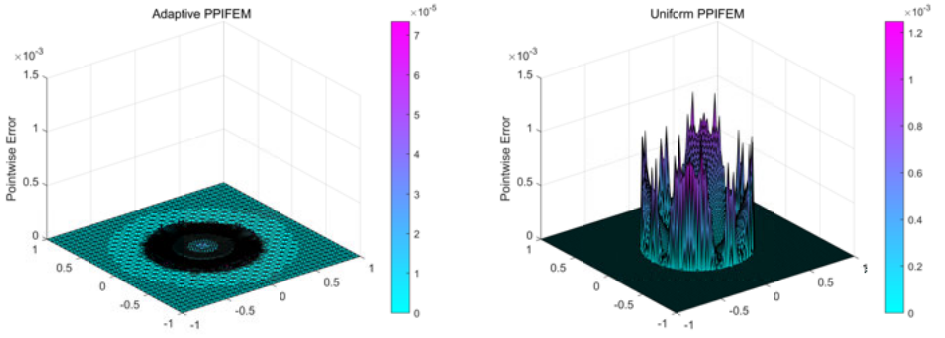


(a) Adaptive meshes (b) Uniform meshes

FIG. 6.4. *The pointwise errors on uniformly and adaptively refined meshes for* $\beta^+/\beta^- = 10^4$.

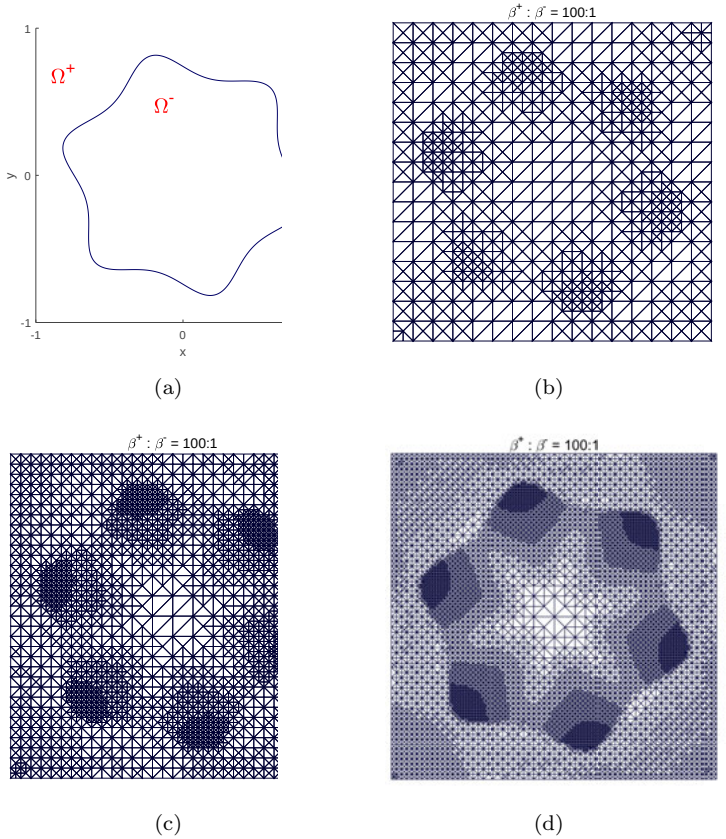


(a) (b)

(c) (d)

FIG. 6.5. *(a) The flower-like interface; (b) Adaptive meshes with* 1320 *triangles on level* 4*; (c) Adaptive meshes with* 4840 *triangles on level* 8*; (d) Adaptive meshes with* 16190 *triangles on level* 12.

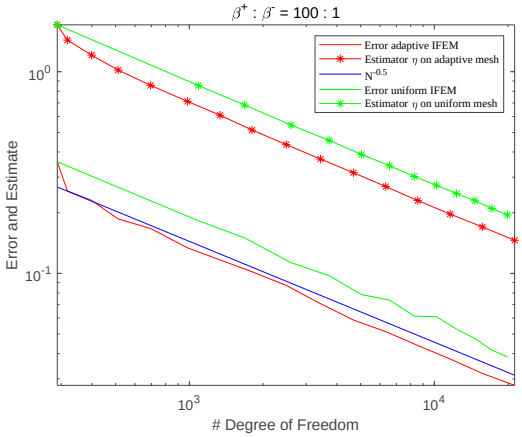


(a) Adaptive meshes

FIG. 6.6. *Convergence of the error and the estimator on uniformly and adaptively refined meshes.*

the previous example. It shows that our error indicator captures the local distribution of the error very well for complex interface geometry.

The convergence graphs of the error $\left\|\alpha^{1/2}\nabla(u-u_\tau)\right\|$ and the estimated error are plotted on both uniform and adaptive meshes in Figure 6.6, together with the theoretical convergence rates $N^{-1/2}$. We can see that the errors on adaptive meshes are smaller than on uniform ones. As in the previous example, the estimator gives an upper bound on the error and they decrease at the same speed. They once again match quite well. This example confirms that a more complicated interface can easily be considered in this framework and that optimal convergence can equally well be done.

The numerical results presented in this section emphasize the reliability and efficiency of the error estimator. Moreover, this confirms that adaptive refinement is more efficient than uniform when solving elliptic interface problems with different interface geometries or different jump ratios.

## 7. Conclusion

This paper derived and analyzed a residual-based a posteriori error estimate for the PPIFE method applied to two-dimensional elliptic interface problems. First, we constructed a robust and computationally simple a posterior error estimator that includes the element residual, the numerical flux jump, and the numerical solution jump. We further demonstrated that the estimator is efficient with constants independent of the jump of the diffusion coefficients across interfaces, the interface location, and the mesh size. A new and direct approach based on an $L^2$ representation of the true error was introduced without involving the Helmholtz decomposition and has been applied to prove that the estimator is reliable. Moreover, we proposed a more local adaptive mesh refinement strategy based on a posterior error estimation and adopted it for the PPIFE method to solve the interface problem. For different jump rates or interface geometries, numerical results verify that the estimator is efficient and reliable and illustrate the improved convergence rate in comparison to uniform mesh-refining. In future work, we will consider residual-based a posteriori error estimates of IFE methods for parabolic interface problems.

**Acknowledgements.** This work is supported by the National Natural Science Foundation of China (41974133, 11971410), State Key Program of National Natural Science Foundation of China (11931003) and Postgraduate Scientific Research Innovation Project of Hunan Province (CX20210606).

## REFERENCES

[1] A. Hansbo and P. Hansbo, *An unfitted finite element method based on Nitsche's method for elliptic interface problems*, Comput. Meth. Appl. Mech. Eng., 191(47-48):5537–5552, 2002. 1
[2] C. Bernardi and R. Verfürth, *Adaptive finite element methods for elliptic equations with non-smooth coefficients*, Numer. Math., 85(4):579–608, 2000. 1
[3] E. Haber and U.M. Ascher, *Fast finite volume simulation of 3D electromagnetic problems with highly discontinuous coefficients*, SIAM J. Sci. Comput., 22(6):1943–1961, 2001. 1
[4] Y. Efendiev and T. Hou, *Multiscale finite element methods for porous media flows and their applications*, Appl. Numer. Math., 57(5-7):577–596, 2007. 1
[5] D. Gueribiz, F. Jacquemin, and S. Fréour, *A moisture diffusion coupled model for composite materials*, Eur. J. Mech. A/Solids, 42:81–89, 2013. 1
[6] J. Xu, *Error estimates of the finite element method for the second order elliptic equations with discontinuous coefficients*, J. Xiangtan. Univ., 1:1–5, 1982. 1
[7] Z. Chen and J. Zou, *Finite element methods and their convergence for elliptic and parabolic interface problems*, Numer. Math., 79(2):175–202, 1998. 1
[8] L. Chen, H. Wei, and M. Wen, *An interface-fitted mesh generator and virtual element methods for elliptic interface problems*, J. Comput. Phys., 334:327–348, 2017. 1
[9] G. Wang, F. Wang, L. Chen, and Y. He, *A divergence free weak virtual element method for the Stokes–Darcy problem on general meshes*, Comput. Meth. Appl. Mech. Eng., 344:998–1020, 2019. 1
[10] L. Mu, J. Wang, G. Wei, X. Ye, and S. Zhao, *Weak Galerkin methods for second order elliptic interface problems*, J. Comput. Phys., 250:106–125, 2013. 1
[11] L. Song, S. Zhao, and K. Liu, *A relaxed weak Galerkin method for elliptic interface problems with low regularity*, Appl. Numer. Math., 128:65–80, 2018. 1
[12] H. Sauerland and T.P. Fries, *The extended finite element method for two-phase and free-surface flows: A systematic study*, J. Comput. Phys., 230(9):3369–3390, 2011. 1
[13] N. Wang and J. Chen, *A nonconforming Nitsche's extended finite element method for Stokes interface problems*, J. Sci. Comput., 81(1):342–374, 2019. 1
[14] R.J. LeVeque and Z. Li, *The immersed interface method for elliptic equations with discontinuous coefficients and singular sources*, SIAM J. Numer. Anal., 31(4):1019–1044, 1994. 1
[15] M. Colnago, W. Casaca, and L.F. de Souza, *A high-order immersed interface method free of derivative jump conditions for Poisson equations on irregular domains*, J. Comput. Phys., 423:109791, 2020. 1
[16] L. Zhang, A. Gerstenberger, X. Wang, and W.K. Liu, *Immersed finite element method*, Comput. Meth. Appl. Mech. Eng., 193(21-22):2051–2067, 2004. 1
[17] X. He, T. Lin, Y. Lin, and X. Zhang, *Immersed finite element methods for parabolic equations with moving interface*, Numer. Meth. Partial Differ. Equ., 29(2):619–646, 2012. 1
[18] T. Lin, D. Sheen, and X. Zhang, *A locking-free immersed finite element method for planar elasticity interface problems*, J. Comput. Phys., 247:228–247, 2013. 1
[19] T. Lin, Y. Lin, and X. Zhang, *A method of lines based on immersed finite elements for parabolic moving interface problems*, Adv. Appl. Math. Mech., 5(04):548–568, 2013. 1
[20] R. Guo, T. Lin, and Y. Lin, *Approximation capabilities of immersed finite element spaces for elasticity interface problems*, Numer. Meth. Partial Differ. Equ., 35(3):1243–1268, 2019. 1
[21] D. Jones and X. Zhang, *A class of nonconforming immersed finite element methods for Stokes interface problems*, J. Comput. Appl. Math., 392:113493, 2021. 1
[22] Y. Wang, Y. Chen, Y. Huang, and Y. Liu, *Two-grid methods for semi-linear elliptic interface problems by immersed finite element methods*, Appl. Math. Mech. Engl. Ed., 40(11):1657–1676, 2019. 1
[23] Z. Li, *The immersed interface method using a finite element formulation*, Appl. Numer. Math., 27(3):253–267, 1998. 1
[24] T. Lin, Y. Lin, and X. Zhang, *Partially penalized immersed finite element methods for elliptic interface problems*, SIAM J. Numer. Anal., 53(2):1121–1144, 2015. 1, 4, 6
[25] T. Lin and Q. Zhuang, *Optimal error bounds for partially penalized immersed finite element methods for parabolic interface problems*, J. Comput. Appl. Math., 366:112401, 2020. 1

[26] Q. Yang, *Numerical analysis of partially penalized immersed finite element methods for hyperbolic interface problems*, Numer. Math. Theory Meth. Appl., 11(2):272–298, 2018. 1
[27] A. Liu and J. Chen, *A partially penalized $P1/CR$ immersed finite element method for planar elasticity interface problems*, Numer. Meth. Partial Differ. Equ., 35(6):2318–2347, 2019. 1
[28] P. Huang and Z. Li, *Partially penalized IFE methods and convergence analysis for elasticity interface problems*, J. Comput. Appl. Math., 382:113059, 2021. 1
[29] Y. Chen and X. Zhang, *A $P2-P1$ partially penalized immersed finite element method for Stokes interface problems*, Int. J. Numer. Anal. Model., 18:120–141, 2021. 1
[30] R. Guo, T. Lin, Y. Lin, and Q. Zhuang, *Error analysis of symmetric linear/bilinear partially penalized immersed finite element methods for Helmholtz interface problems*, J. Comput. Appl. Math., 390:113378, 2021. 1
[31] Z. Chen, Y. Xiao, and L. Zhang, *The adaptive immersed interface finite element method for elliptic and Maxwell interface problems*, J. Comput. Phys., 228(14):5000–5019, 2009. 1
[32] C. He and X. Zhang, *Residual-based a posteriori error estimation for immersed finite element methods*, J. Sci. Comput., 81(3):2051–2079, 2019. 1, 4, 4, 4, 5, 5.1
[33] R. Verfürth, *A review of a posteriori error estimation techniques for elasticity problems*, Comput. Meth. Appl. Mech. Eng., 176(1-4):419–440, 1999. 1
[34] Z. Li, T. Lin, and X. Wu, *New cartesian grid methods for interface problems using the finite element formulation*, Numer. Math., 96(1):61–98, 2003. 2.2
[35] Z. Li, T. Lin, Y. Lin, and R.C. Rogers, *An immersed finite element space and its approximation capability*, Numer. Meth. Partial Differ. Equ., 20(3):338–367, 2004. 2.2
[36] R. Verfürth, *A posteriori error estimation and adaptive mesh-refinement techniques*, J. Comput. Appl. Math., 50(1-3):67–83, 1994. 3.1, 4
[37] M. Ainsworth and J. Oden, *A posteriori error estimation in finite element analysis*, Comput. Meth. Appl. Mech. Eng., 142(1-2):1–88, 1997. 3.1
[38] C. Bernardi and R. Verfürth, *Adaptive finite element methods for elliptic equations with non-smooth coefficients*, Numer. Math., 85(4):579–608, 2000. 4, 4
[39] Z. Cai, C. He, and S. Zhang, *Discontinuous finite element methods for interface problems: Robust a priori and a posteriori error estimates*, SIAM J. Numer. Anal., 55(1):400–418, 2017. 5
[40] L. T. Huynh, N. Nguyen, J. Peraire, and B. Khoo, *A high-order hybridizable discontinuous Galerkin method for elliptic interface problems*, Int. J. Numer. Meth. Eng., 93(2):183–200, 2012. 6
[41] R. Guo, T. Lin, and X. Zhang, *Nonconforming immersed finite element spaces for elliptic interface problems*, Comput. Math. Appl., 75(6):2002–2016, 2018. 6
[42] L. Chen, *iFEM: an innovative finite element method package in Matlab*, 2008. 6